ChemComm

COMMUNICATION

An efficient polymeric micromotor doped with Pt nanoparticle@carbon nanotubes for complex bio-media†

Yana Li, Jie Wu,* Yuzhe Xie and Huangxian Ju

Cite this: *Chem. Commun.*, 2015, 51, 6325

Received 20th January 2015,
Accepted 3rd March 2015

DOI: 10.1039/c5cc00546a

www.rsc.org/chemcomm

A highly efficient polymeric tubular micromotor doped with Pt nanoparticle@carbon nanotubes is fabricated by template-assisted electrochemical growth. The micromotors preserve good navigation in multi-media and surface modification, along with simple synthesis, easy functionalization and good biocompatibility, displaying great promise in biological applications.

Recent advancements of nanotechnology promote the development of artificial micro/nanomotors that are able to convert energy into autonomous movements. These micro/nanomotors show different architectures, such as segmented nanowires,[1] conical microtubes,[2] Janus microspheres[3] and some irregular structures,[4] and are propelled along different propulsion mechanisms, including bubble ejection,[2,5] self-diffusiophoresis,[6] self-electrophoresis,[1a] pH gradients,[7] magnetic fields,[8] and ultrasound propulsion.[9] Due to the unique autonomous motion performance and flexible controllability, they have been used in bacterial isolation,[10] drug delivery,[11] sewage purification,[12] microsurgery,[9c] active biomimetic systems,[13] and environmental monitoring.[14] Among these motors, the catalytic motors propelled by bubble-induced propulsion are particularly attractive owing to their efficient movement in ionic-strength solution.[15]

The bubble-induced propulsion relies on the asymmetry of chemical reactions occurring on the tubular motor structures, which are generally prepared by the rolled-up technique[2c,5a,16] or template-assisted assembly/deposition.[17] These motors normally contain outer inert material and inner catalytic Pt coating. The latter can decompose hydrogen peroxide fuel to produce the oxygen bubbles.[5a,17] To extend the application of tubular motors, polymeric materials have been introduced to the catalytic motors due to their good biocompatibility, easy synthesis and functionalization, and nice flexibility. For example, several polymer–metal bilayer micromotors have been prepared by the template-based electrochemical synthesis and used to transport, isolate and detect various biomolecules.[9a,18] A polymer multilayer tubular nanomotor containing Pt nanoparticles (PtNP) in the interior has also been proposed with a template-assisted layer-by-layer assembly technology.[17a] More recently, a microjet with a temperature-responsible polymer as the outer layer has been prepared by the rolled-up technique.[19] Although these polymeric motors show favourable functionalities, they still have some inherent limitations due to the metallic inner layer, which leads to the loss of motion performance in the protein-rich system or the surface passivation of the inner layer in micromotor functionalization with receptors. Therefore the application of catalytic motors still remains a challenge.

Here we describe a bilayer polymeric tubular micromotor prepared by a template-assisted electro-deposition technique. The tubular outer layer of poly(3,4-ethylenedioxythiophene) (PEDOT) is firstly electrochemically synthesized to further co-deposit polypyrrole (PPy) and PtNPs loaded carbon nanotubes (PtNP@CNTs) on its inner wall. The polymeric inner layer not only retains the efficient catalytic ability of PtNPs for obtaining fast movement, but also provides good biocompatibility for avoiding the limitations of previously reported catalytic motors in biological systems. In addition, this is the first example to incorporate CNTs for the loading of PtNPs in the inner layer of the micromotor. The presence of CNTs greatly improves the catalytic activity, which leads to faster movement of the micromotor than those with PtNPs interior.[17a] Due to the protection of porous PPy film, the PEDOT/PtNP@CNT-PPy micromotor possesses good resistance to protein/molecule-induced blocking and poisoning. Fe_3O_4 nanoparticles can also be conveniently co-deposited in PtNP@CNT-PPy to achieve the magnetically directed movement. Thus such a polymeric micromotor shows great promise for diverse applications.

The bilayer PEDOT/PtNP@CNT-PPy micromotor was synthesized by sequential electrochemical growth of PEDOT and PtNP@CNT-PPy on a cyclopore polycarbonate membrane (Scheme 1). Briefly, PEDOT was firstly electropolymerized on the inner wall of the micropores. After PtNP@CNT dispersion was filled into the PEDOT-coated micropores, electrochemical plating was performed in pyrrole solution to rapidly form a PtNP@CNT-PPy layer on the

State Key Laboratory of Analytical Chemistry for Life Science, School of Chemistry and Chemical Engineering, Nanjing University, Nanjing 210093, P.R. China. E-mail: wujie@nju.edu.cn

† Electronic supplementary information (ESI) available: Experimental details and additional figures. See DOI: 10.1039/c5cc00546a

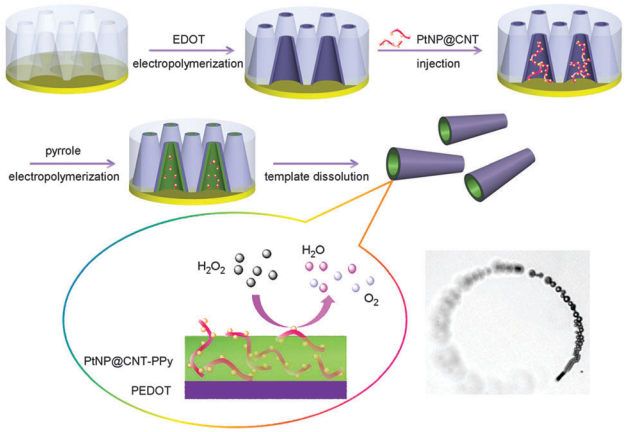

Scheme 1 Schematic illustration of polymeric micromotor fabrication *via* template-assisted electrochemical deposition and a propulsion mechanism.

PEDOT surface. Finally, the polymeric tubular micromotors were obtained after the template dissolution in methylene chloride. In the fuel solution of H_2O_2, oxygen gas could be catalytically produced to propel the movement of the micromotors.

The PtNP@CNTs were prepared by electrostatic assembly of PtNPs on CNTs with the help of a positively charged polyelectrolyte (ESI†). Compared with bare CNTs, many individual "nanodots" with an average diameter of 2 nm could be observed on the surface of CNTs after the loading of PtNPs (Fig. S1, ESI†). The top-view SEM image of the PEDOT/PtNP@CNT-PPy micromotor showed a length of ~12 μm and a defined cone tubular geometry with outer diameters of 5 and 4 μm, along with inner openings of 3.8 and 2.8 μm (Fig. 1a). The outer surface of the polymeric microtube was uniform and compact, while the inner surface of PtNP@CNT-PPy was rough (Fig. 1b). The energy-dispersive X-ray (EDX) spectra clearly showed the presence of platinum within the microtube with a uniform distribution (Fig. 1c and d), indicating the successful synthesis of PEDOT/PtNP@CNT-PPy micromotors.

The motion performance of the micromotors depended on the preparation conditions such as the electropolymerization charge and PtNP@CNT concentration. As expected, with increasing the deposition charge more PtNP@CNT-PPy was electropolymerized on the inner wall of PEDOT (Fig. S2a–d, ESI†). When the deposition charge was more than 0.1 C, the thickness of the formed

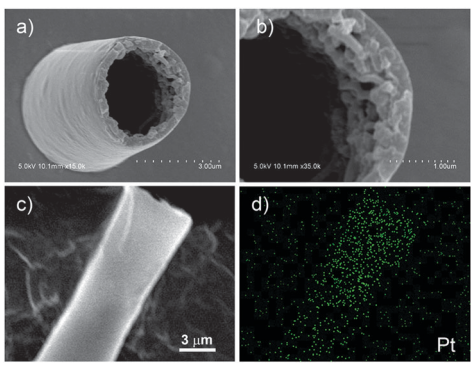

Fig. 1 SEM (a), enlarged SEM (b) and EDX mapping analysis of Pt (c, d) in a PEDOT/PtNP@CNT-PPy micromotor.

PtNP@CNT-PPy layer affected the inner opening diameter, which led to the lower navigation speed of the micromotors in H_2O_2 solution (Fig. S2e, ESI†). Thus, 0.1 C was used for the electropolymerization of the PtNP@CNT-PPy layer. As the motion of the micromotors relied on the catalytic generation of oxygen gas by PtNP@CNTs, the effect of PtNP@CNT concentration was examined (Fig. S2f, ESI†), in which the speed reached the maximum value and trended to the plateau at 200 μg mL^{-1}. Here, the disappeared colour bars in Fig. S2e and f (ESI†) referred to the ultraslow movement of the micromotors under their corresponding experimental conditions.

The composition of the inner polymeric layer was an important factor affecting the motion performance of micromotors. Under the same deposition conditions, the inner layer formed by PPy (PtNP@CNT-PPy) showed much more PtNP@CNTs, which were arrowed in Fig. S3, ESI† in the polymer than that by polyaniline (PtNP@CNT-PANI), and a more uniform surface than that by PEDOT (PtNP@CNT-PEDOT) (Fig. S3, ESI†). This result was further confirmed by the EDX mapping analysis (Fig. 1c,d, Fig. S4a–d and Table S1, ESI†). The presence of platinum (25.80%) in the micromotor with the PtNP@CNT-PPy inner layer was much more than those of 18.91% and 8.83% in micromotors with PtNP@CNT-PEDOT and PtNP@CNT-PANI inner layers, respectively, suggesting that more PtNP@CNTs could be deposited within the PPy layer. The more PtNP@CNTs led to stronger catalytic activity of the inner layer to decompose hydrogen peroxide fuel and thus resulted in faster navigation speed, while the uniform PtNP@CNT-PPy layer was also beneficial to the motion performance. Thus the PEDOT/PtNP@CNT-PPy micromotor displayed a navigation speed of 288 μm s^{-1}, faster than 0 and 138 μm s^{-1} of PEDOT/PtNP@CNT-PANI and PEDOT/PtNP@CNT-PEDOT micromotors at 5% H_2O_2, respectively (Video S1, ESI†).

The efficient propulsion of the PEDOT/PtNP@CNT-PPy micromotor was illustrated in Fig. 2. A tail of oxygen bubbles generated from the catalytic decomposition of H_2O_2 by the PtNP@CNT-PPy inner layer were released from the rear large-opening side of the micromotor, which offered an average speed of 143 μm s^{-1} (nearly 12 body lengths) (Video S2, ESI†). The drag force of the micromotor could be estimated to be 10 pN using the Stokes' drag theory,[2a]

$$F_d = \frac{2\pi\mu LU}{\ln(L/a) - 1/2}$$

where F_d is the fluid resistance, U is the speed of the micromotor (143 μm s^{-1}), μ is the fluid dynamic viscosity (1.01 mPa s, equal to 1.01×10^{-3} N m^{-2} s), L is the length (12 μm) and a is the radius (2.5 μm) of the micromotor. Such a speed was stable for at least 20 min. In contrast, no motion performance was observed in the absence of CNTs for PEDOT/PtNP-PPy or PtNPs for PEDOT/CNT-PPy (Video S3, ESI†), indicating the efficient catalytic ability of PtNP@CNTs in the PPy layer. Here, the poor motion performance of the PEDOT/PtNP-PPy micromotor could be attributed to the too low amount of PtNPs codeposited in the PPy layer (Fig. S4e,f and Table S1, ESI†).

The speed of the PEDOT/PtNP@CNT-PPy micromotors depended on the concentration of H_2O_2 fuel. Their average speed increased from 62 ± 15 μm s^{-1} (nearly 5 body lengths) at

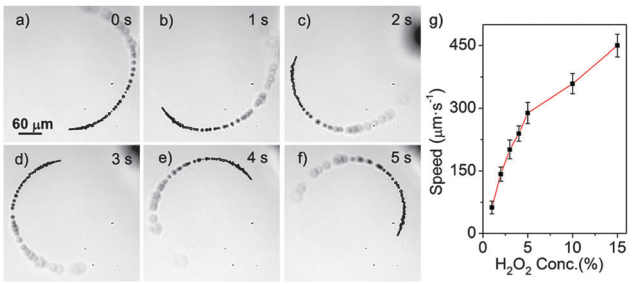

Fig. 2 (a)–(f) Time-lapse motion images of a PEDOT/PtNP@CNT-PPy micromotor in 2% H_2O_2 solution containing 1.6% (w/v) sodium cholate, and (g) dependence of average speed on H_2O_2 concentration. Error bars represented the standard deviations of speed from 20 micromotors.

1% H_2O_2 to 450 ± 26 μm s^{-1} (nearly 35 body lengths) at 15% H_2O_2, in the presence of 1.6% (w/v) sodium cholate (Fig. 2g and Video S2, ESI†). This tendency was primarily related to the bubble generation frequency. Compared with 5 and 70 μm s^{-1} at 1% and 15% H_2O_2 for layer-by-layer assembled polymer–PtNP motors,[17a] the present PEDOT/PtNP@CNT-PPy micromotors displayed much higher motion speed in the studied concentration range of H_2O_2, suggesting the good catalytic activity of PtNP@CNTs. It was attributed to the high surface area of CNTs for loading more PtNPs in the inner layer. In addition, the CNTs might also enhance the catalytic ability of PtNPs due to their synergistic action.[20]

Remote control of the micromotors using an external field is of utmost importance since it allows the motors with directed movement to realize some essential functions, such as drug delivery and targeted therapy.[21] Here, the magnetic guidance of PEDOT/PtNP@CNT-PPy micromotors could be conveniently achieved by co-depositing Fe_3O_4 nanoparticles in the PtNP@CNT-PPy layer (Fig. S5, ESI†). The corresponding video (Video S4, ESI†) displayed that the Fe_3O_4 nanoparticles doped micromotors could navigate along the predetermined (*N*, *J*, *U*) trajectories at a constant speed in an external magnetic field.

The motion performance of the catalytic motors commonly suffers great loss in protein-rich systems or after motor modification with receptors owing to the surface passivation of the Pt layer,[22] which limits their practical application in biological systems. Due to the protection of porous PPy film, the proposed micromotors showed an ability to preserve the catalytic activity of PtNP@CNTs against protein/molecule-induced blocking and poisoning. Different from the PEDOT/Pt micromotors,[23] whose speed and the bubble generation frequency decreased sharply with the increase of bovine serum albumin (BSA) concentration and then trended to 0 at 500 μM BSA, the motion performance of PEDOT/PtNP@CNT-PPy micromotors could be maintained with BSA concentration lower than 10 μM, and showed gentle speed loss in the BSA concentration from 10 to 500 μM (Fig. 3 and Video S5, ESI†). Even in the BSA concentration high to 1000 μM, the PEDOT/PtNP@CNT-PPy micromotors still retained good navigation with a speed of 52 ± 15 μm s^{-1} at 2% H_2O_2. Here, the decrease of motion speed of PEDOT/PtNP@CNT-PPy micromotors was mainly attributed to the increased viscosity from the high-concentration BSA. The good motion performance of PEDOT/PtNP@CNT-PPy micromotors in the protein-rich

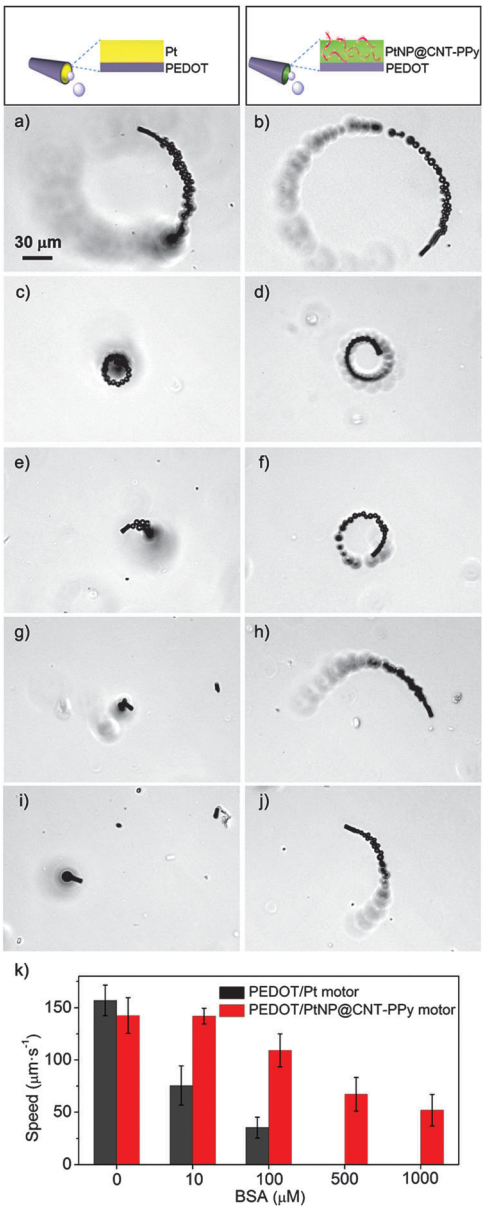

Fig. 3 (a)–(j) Time-lapse images of PEDOT/Pt (a, c, e, g, i) and PEDOT/PtNP@CNT-PPy (b, d, f, h, j) micromotors in BSA solutions at 0 (a, b), 10 (c, d), 100 (e, f) 500 (g, h) and 1000 (i, j) μM, respectively, containing 2% H_2O_2 and 1.6% (w/v) sodium cholate. (k) Dependence of average speeds of PEDOT/Pt and PEDOT/PtNP@CNT-PPy micromotors on BSA concentration. Error bars represented the standard deviations of speed from 20 micromotors.

system showed important applications of the catalytic micromotors in complex bio-media.

The polymeric micromotors showed good motion performance in different media. For example, they displayed a motion speed of 140 ± 18 μm s^{-1} in 0.1 M KCl solution containing 2% H_2O_2, which was similar as that in water (Fig. S6a and Video S6, ESI†), suggesting that the motor movement was salt-independent. Similar to the low speed in the protein-rich system, the micromotors displayed circular motion with the speeds of 77 ± 11 and 66 ± 10 μm s^{-1} in human serum and cell culture medium, respectively, due to the viscosity effect.

In order to evaluate the practical application of the polymeric micromotor, wheat germ agglutinin (WGA) modified PEDOT/PtNP@CNT-PPy micromotors were prepared to capture and isolate pathogenic gram-negative bacteria (*E. coli*) in Luria-Bertani broth containing 2% H_2O_2. The modification of WGA was performed through the electrostatic assembly of AuNPs on PEDOT and then WGA on AuNPs.[24] The WGA modified PEDOT/PtNP@CNT-PPy micromotors displayed a motion speed of 138 μm s^{-1} in 2% H_2O_2 (Fig. S7a and Video S7, ESI†). Apparently, the modification procedure did not affect the propulsion of the proposed polymeric micromotors (Fig. S6b, ESI†), which was superior to 47% and 92% of the speed decrease upon bio-modification of PANI/Pt[10] and rolled-up[15c] motors. Based on the specific recognition of lectin to glycan, the WGA modified PEDOT/PtNP@CNT-PPy micromotor could be used to recognize, capture and isolate *E. coli* (Fig. S7c and Video S7, ESI†). In contrast, no successful capture could be observed in the unmodified micromotors (Fig. S7b, ESI†).

In conclusion, we have demonstrated a new and vigorous polymeric tubular micromotor prepared by template-assisted electropolymerization of PEDOT as the outer layer and PtNP@CNT-PPy as the inner catalyst layer. The PEDOT/PtNP@CNT-PPy micromotors show excellent motion performance in low-level fuel due to the high catalytic activity of PtNP@CNTs and in bio-related environments including the protein-rich system due to the protection of porous PPy film. The magnetically directed movement of the micromotors has been achieved by co-depositing Fe_3O_4 nanoparticles in the polymeric inner layer. Furthermore, the loss of motion speed during the bio-functionalization of the micromotors can be avoided. After the outer surface is modified with WGA, the polymeric micromotors can autonomously recognize, capture and transport pathogenic bacteria *E. coli* in biological environment. The simple and mass preparation, easy modification, good biocompatibility and excellent navigation performance in complex media indicate the great promise of the polymeric micromotors in biological applications.

This work was supported by National Natural Science Foundation of China (21105046, 21135002 and 21121091), PhD Fund for Young Teachers (20110091120012), and Natural Science Foundation of Jiangsu (BK2011552).

Notes and references

1 (*a*) W. F. Paxton, K. C. Kistler, C. C. Olmeda, A. Sen, S. K. St. Angelo, Y. Cao, T. E. Mallouk, P. E. Lammert and V. H. Cresp, *J. Am. Chem. Soc.*, 2004, **126**, 13424–13431; (*b*) S. Fournier-Bidoz, A. C. Arsenault, I. Manners and G. A. Ozin, *Chem. Commun.*, 2005, 441–443; (*c*) R. Liu and A. Sen, *J. Am. Chem. Soc.*, 2011, **133**, 20064–20067; (*d*) W. Wang, W. T. Duan, A. Sen and T. E. Mallouk, *Proc. Natl. Acad. Sci. U. S. A.*, 2013, **44**, 17744–17749.

2 (*a*) W. Gao, S. Sattayasamitsathit, J. Orozco and J. Wang, *J. Am. Chem. Soc.*, 2011, **133**, 11862–11864; (*b*) W. Gao, A. Uygun and J. Wang, *J. Am. Chem. Soc.*, 2012, **134**, 897–900; (*c*) A. A. Solovev, Y. F. Mei, E. B. Ureña, G. S. Huang and O. G. Schmidt, *Small*, 2009, **5**, 1688–1692.

3 (*a*) R. A. Pavlick, S. Sengupta, T. McFadden, H. Zhang and A. Sen, *Angew. Chem., Int. Ed.*, 2011, **50**, 9374–9377; (*b*) F. Z. Mou, C. R. Chen, H. R. Ma, Y. X. Yin, Q. Z. Wu and J. G. Guan, *Angew. Chem., Int. Ed.*, 2013, **52**, 1–6; (*c*) W. Gao, A. Pei, R. F. Dong and J. Wang, *J. Am. Chem. Soc.*, 2014, **136**, 2276–2279.

4 (*a*) B. Dong, T. Zhou, H. Zhang and C. Y. Li, *ACS Nano*, 2013, **7**, 5192–5198; (*b*) H. Wang, G. J. Zhao and M. Pumera, *J. Am. Chem. Soc.*, 2014, **136**, 2719–2722; (*c*) D. A. Wilson, R. J. M. Nolte and J. C. M. van Hest, *Nat. Chem.*, 2012, **4**, 268–274.

5 (*a*) A. A. Solovev, S. Sanchez, M. Pumera, Y. F. Mei and O. G. Schmidt, *Adv. Funct. Mater.*, 2010, **20**, 2430–2435; (*b*) J. Wang and W. Gao, *ACS Nano*, 2012, **6**, 5745–5751.

6 (*a*) M. N. Popescu, S. Dietrich, M. Tasinkevych and J. Ralston, *Eur. Phys. J. E: Soft Matter Biol. Phys.*, 2010, **31**, 351–367; (*b*) R. Golestanian, T. B. Liverpool and A. Ajdari, *New J. Phys.*, 2007, **9**, 1–8; (*c*) M. Ibele, T. E. Mallouk and A. Sen, *Angew. Chem., Int. Ed.*, 2009, **48**, 3308–3312; (*d*) Y. Y. Hong, M. Diaz, U. M. Córdova-Figueroa and A. Sen, *Adv. Funct. Mater.*, 2010, **20**, 1568–1576; (*e*) D. Kagan, S. Balasubramanian and J. Wang, *Angew. Chem., Int. Ed.*, 2011, **50**, 503–506.

7 K. K. Dey, S. Bhandari, D. Bandyopadhyay, S. Basu and A. Chattopadhyay, *Small*, 2013, **9**, 1916–1920.

8 (*a*) L. Zhang, T. Petit, K. E. Peyer and B. J. Nelson, *Nanomed.: Nanotechnol., Biol. Med.*, 2012, **8**, 1074–1080; (*b*) L. Zhang, J. J. Abbott, L. X. Dong, K. E. Peyer, B. E. Kratochvil, H. X. Zhang, C. Bergeles and B. J. Nelson, *Nano Lett.*, 2009, **9**, 3663–3667.

9 (*a*) V. Garcia-Gradilla, J. Orozco, S. Sattayasamitsathit, F. Soto, F. Kuralay, A. Pourazary, A. Katzenberg, W. Gao, Y. F. Shen and J. Wang, *ACS Nano*, 2013, **7**, 9232–9240; (*b*) W. Wang, L. A. Castro, M. Hoyos and T. E. Mallouk, *ACS Nano*, 2012, **6**, 6122–6132; (*c*) D. Kagan, M. J. Benchimol, J. C. Claussen, E. Chuluun-Erdene, S. Esener and J. Wang, *Angew. Chem., Int. Ed.*, 2012, **51**, 7519–7522.

10 S. Campuzano, J. Orozco, D. Kagan, M. Guix, W. Gao, S. Sattayasamitsathit, J. C. Claussen, A. Merkoçi and J. Wang, *Nano Lett.*, 2012, **12**, 396–401.

11 Y. J. Wu, Z. G. Wu, X. K. Lin, Q. He and J. B. Li, *ACS Nano*, 2012, **6**, 10910–10916.

12 (*a*) M. Guix, J. Orozco, M. García, W. Gao, S. Sattayasamitsathit, A. Merkoçi, A. Escarpa and J. Wang, *ACS Nano*, 2012, **6**, 4445–4451; (*b*) J. Orozco, G. Z. Cheng, D. Vilela, S. Sattayasamitsathit, R. Vazquez-Duhalt, G. Valdés-Ramírez, O. S. Pak, A. Escarpa, C. Y. Kan and J. Wang, *Angew. Chem., Int. Ed.*, 2013, **52**, 13276–13279.

13 T. Mirkovic, N. S. Zacharia, G. D. Scholes and G. A. Ozin, *Small*, 2010, **6**, 159–167.

14 J. Orozco, V. García-Gradilla, M. D'Agostino, W. Gao, A. Cortés and J. Wang, *ACS Nano*, 2013, **7**, 818–824.

15 (*a*) G. S. Huang, J. Wang and Y. F. Mei, *J. Mater. Chem.*, 2012, **22**, 6519–6525; (*b*) W. Gao, S. Sattayasamitsathit and J. Wang, *Chem. Rec.*, 2012, **12**, 224–231; (*c*) S. Balasubramanian, D. Kagan, C. J. Hu, S. Campuzano, M. J. Lobo-Castañon, N. Lim, D. Y. Kang, M. Zimmerman, L. F. Zhang and J. Wang, *Angew. Chem., Int. Ed.*, 2011, **50**, 4161–4164.

16 Y. F. Mei, A. A. Solovev, S. Sanchez and O. G. Schmidt, *Chem. Soc. Rev.*, 2011, **40**, 2109–2119.

17 (*a*) Z. G. Wu, Y. J. Wu, W. P. He, X. K. Lin, J. M. Sun and Q. He, *Angew. Chem., Int. Ed.*, 2013, **52**, 7000–7003; (*b*) K. M. Manesh, M. Cardona, R. Yuan, M. Clark, D. Kagan, S. Balasubramanian and J. Wang, *ACS Nano*, 2010, **4**, 1799–1804; (*c*) G. J. Zhao, A. Ambrosi and M. Pumera, *Nanoscale*, 2013, **5**, 1319–1324.

18 (*a*) J. Wu, S. Balasubramanian, D. Kagan, K. M. Manesh, S. Campuzano and J. Wang, *Nat. Commun.*, 2010, **1**, 36; (*b*) J. Orozco, A. Cortés, G. Z. Cheng, S. Sattayasamitsathit, W. Gao, X. M. Feng, Y. F. Shen and J. Wang, *J. Am. Chem. Soc.*, 2013, **135**, 5336–5339.

19 V. Magdanz, G. Stoychev, L. Ionov, S. Sanchez and O. G. Schmidt, *Angew. Chem., Int. Ed.*, 2014, **53**, 2673–2677.

20 (*a*) F. L. Qu, M. H. Yang, G. L. Shen and R. Q. Yu, *Biosens. Bioelectron.*, 2007, **22**, 1749–1755; (*b*) Y. X. Fang, D. Zhang, X. Qin, Z. Y. Miao, S. Takahashi, J. Anzai and Q. Chen, *Electrochim. Acta*, 2012, **70**, 266–271.

21 (*a*) W. Gao, D. Kagan, O. S. Pak, C. Clawson, S. Campuzano, E. Chuluun-Erdene, E. Shipton, E. E. Fullerton, L. F. Zhang, E. Lauga and J. Wang, *Small*, 2012, **8**, 460–467; (*b*) D. Kagan, R. Laocharoensuk, M. Zimmerman, C. Clawson, S. Balasubramanian, D. Kang, D. Bishop, S. Sattayasamitsathit, L. F. Zhang and J. Wang, *Small*, 2010, **6**, 2741–2747.

22 (*a*) C. H. Bartholomew, P. K. Agrawal and J. R. Katzer, *Adv. Catal.*, 1982, **31**, 135–242; (*b*) H. Elwing, *Biomaterials*, 1998, **19**, 397–406; (*c*) V. H. L. Lee and A. Yamamoto, *Adv. Drug Delivery Rev.*, 1989, **4**, 171–207.

23 W. Gao, S. Sattayasamitsathit, A. Uygun, A. Pei, A. Ponedal and J. Wang, *Nanoscale*, 2012, **4**, 2447–2453.

24 X. P. Yu, Y. N. Li, J. Wu and H. X. Ju, *Anal. Chem.*, 2014, **86**, 4501–4507.

